The Effect of Surfactants on Surface-Induced Denaturation of Proteins: Evidence of an Orientation-Dependent Mechanism

Andrea Arsiccio,[†] James McCarty,[‡] Roberto Pisano,[†] and Joan-Emma Shea[*,‡,¶]

Department of Applied Science and Technology, Politecnico di Torino, 24 corso Duca degli Abruzzi, Torino 10129, Italy, Department of Chemistry and Biochemistry, University of California, Santa Barbara, California 93106, United States, and Department of Physics, University of California, Santa Barbara, California 93106, United States

E-mail: shea@ucsb.edu

[*]To whom correspondence should be addressed

[†]Department of Applied Science and Technology, Politecnico di Torino, 24 corso Duca degli Abruzzi, Torino 10129, Italy

[‡]Department of Chemistry and Biochemistry, University of California, Santa Barbara, California 93106, United States

[¶]Department of Physics, University of California, Santa Barbara, California 93106, United States

Abstract

When proteins bind to interfaces, the resulting changes in protein structure can lead to loss of protein function. We investigate the mechanism by which surfactant molecules can counteract surface-induced protein denaturation through a detailed study of the stability of the GB1 peptide at the air-water, ice-water and silica-water interfaces using molecular dynamics simulations coupled with metadynamics. Our simulations reveal that the air-water interface, and to a lesser extent the ice-water interface, destabilize the protein by direct interactions between the protein and surface that disrupt the hydrophobic core of the protein, while the weakly-interacting silica surface stabilizes the protein through confinement effects. Addition of the surfactant Tween 80 leads to stabilization of the protein at the air-water and ice-water surfaces, and mild destabilization at the water-silica interface. We show that the amphiphilic nature of the surfactant is key to its stabilizing/destabilizing effect, with an orientation-dependent mechanism in which the protein is stabilized when the hydrophilic heads of the surfactant point toward the protein.

Keywords

Protein adsorption, Surfactants, Metadynamics, Surfaces

Introduction

The biological activity of a globular protein is intimately tied to its three-dimensional folded structure. Proteins are marginally stable, and chemical and thermal changes in the environment can readily affect their conformations, and hence, their ability to perform their function. The cell has evolved a host of mechanisms to ensure that proteins remain functional, including the use of chaperones and osmolytes.

Although *in vitro* environments are considerably simpler than the cell, and thermal and chemical composition can be controlled, an issue that becomes prevalent is surface-induced

protein adsorption and denaturation. Surfaces are present in most *in vitro* experiments: the glass container of a test tube, inorganic or organic surfaces used in biosensors, and even the air-water interface. Surface-induced denaturation can have serious consequences in the field of pharmacology, where loss of protein native structure leads to loss of drug activity, and can even lead to a fatal immune response in the patient.

Drawing from the cell's defense mechanism against protein denaturation, one can mitigate protein denaturation *in vitro* through addition of protective osmolytes, or surfactant molecules. Surfactant molecules are a particularly attractive means, as these molecules are readily synthesized and have been shown to counter surface-induced denaturation in a number of studies. Surfactants are amphipathic molecules, with a hydrophobic tail and an anionic, cationic, or non-ionic hydrophilic head. Non-ionic surfactants, and, among these, the polysorbates Tween 20 or Tween 80, are commonly used in pharmaceutical studies to stabilize protein-based drugs in experiments where surface-induced denaturation is an issue.

While surfactants are used routinely, the mechanism by which they prevent surface-induced denaturation of proteins is poorly understood. It has been hypothesized that surfactants bind to the surface, forming a protective layer and thereby preventing protein adsorption, and hence denaturation. Alternately, it has also been suggested that the surfactants interact with the protein in solution, in this way screening protein interaction with the surface.

In this study, we use atomistic molecular dynamics (MD) simulations to investigate the effect of surfactants in preventing surface-induced protein denaturation. MD simulation can complement experimental studies by elucidating transiently populated intermediate conformational states as well as unfolding pathways. However, protein conformational transitions typically take place on timescales longer than those that can be feasibly simulated with conventional MD, and obtaining information regarding important transient states requires exhaustive sampling of the configurational state space. To overcome this limitation we employ the metadynamics enhanced sampling method.[1,2] Metadynamics significantly reduces

the amount of computational time needed to obtain a meaningful statistical sampling of configuration space by introducing a history-dependent bias potential that acts on a set of relevant order parameters or collective variables (CVs). In the context of protein adsorption, the efficacy of metadynamics largely depends on a judicious choice of CVs, which can include the distance between the surface and the protein center-of-mass, various metrics of protein secondary structure, and the coordination of surfactant molecules with either the protein or surface. To account for as many CVs as needed we use a variant of metadynamics called parallel bias metadynamics[3] (PBMetaD) introduced by Pfaendtner and Bonomi. PBMetaD alleviates the difficulty of depositing a high-dimensional bias by instead constructing multiple one-dimensional biases each acting on a single CV in parallel. This approach, and molecular dynamics in general, have been successfully applied to study protein-surface interactions.[4–9]

We use the GB1 hairpin and Tween 80 as model protein and surfactant, and we consider the air-water, ice-water and silica-water interfaces. The GB1 peptide (shown in Figure 1a) corresponds to residues 41-56 of the GB1 protein.

The GB1 peptide is well-studied both experimentally and computationally,[10–21] and has been shown to robustly fold to a stable structure in a number of MD force fields. In earlier work, we studied the folding of this protein in the presence of self-assembled monolayers and graphite-like surfaces.[22] An important result from our work was that specific interactions between the surface and the protein determine whether or not a protein will unfold at an interface, and that these interactions are more dominant than general considerations of surface hydrophobicity or hydrophilicity. In particular, we showed that two chemically different surfaces with the same hydrophobicity/philicity stabilize/denature the protein to different extents.

Our model surfactant is Tween 80 (Figure 1b), a polysorbate (a molecule consisting of a sorbitan ring with poly(ethylene oxide) at the hydroxyl positions). The polysorbates have been shown experimentally to reduce surface-induced denaturation and aggregation,[23–26] and, recently, their effect on protein conformational stability in the bulk was also compu-

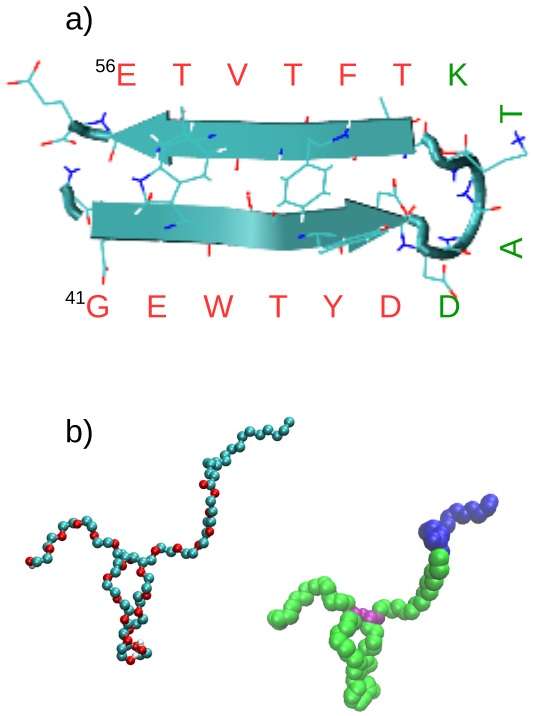

Figure 1: Illustration of a) the GB1 hairpin and b) the Tween 80 molecule. In panel a), the GB1 sequence is also shown, with the β strand residues in red, and those in green being part of the turn. In panel b), two different representations of Tween 80 are shown. On the left, the carbon atoms are shown in blue, and the oxygen ones in red. On the right, the hydrophilic poly(ethylene oxide) head groups X, Y, Z and W of Tween 80 are colored in green, while the tail is represented in blue. The central purple group is the sorbitan ring.

tationally investigated.[27] The air-, ice- and silica-water surfaces were chosen because they are relevant in biotechnology settings, and they differ in hydrophobicity and in their ability to bind to proteins. The air-water interface is the most common hydrophobic interface encountered by proteins in a laboratory setting, particularly during stirring or shaking of the solution.[28,29] The ice-water interface is relevant for freeze-drying processes, with the surface of ice an agent for loss of protein activity.[25,30] Silica interfaces are relevant as proteins *in vitro* are exposed to the glass surfaces of beakers, syringes (for drug delivery), and other containers. An understanding of the mechanism by which surfactants counteract the denaturation of proteins at these surfaces would therefore have practical applications in the realm of the pharmaceutical and the biotechnology industry.

In the present work, we investigate the folding of the GB1 hairpin in the bulk, at different surfaces, and in the presence and absence of surfactants. Our simulations reveal that the extent to which surfactants prevent denaturation is dependent on the nature of the surface, and uncover a surfactant orientation-dependent stabilization mechanism in which the surfactant stabilizes the native fold by surrounding the protein with its hydrophilic heads pointing toward the protein.

Materials and Methods

Simulation Details

We simulated the GB1 hairpin in aqueous bulk solvent, and at the vacuum-water, ice-water, and silica-water interfaces, both in the presence and absence of the surfactant Tween 80. All simulations were performed using Gromacs 5.1.4[31] patched with the Plumed 2.4.1 plug-in[32] using the GROMOS53A6 force field[33] for the protein and the GROMOS53A6$_{OXY+D}$ force field[34] for the surfactant. An initial structure for GB1 was taken from the PDB (PDB ID: 1GB1[35]), while the topology file for Tween 80 was obtained from Tang et al.[36]

Tween 80 has four hydrophilic poly(ethylene oxide) head groups (represented in green in

Figure 1b), named X, Y, Z and W heads, which contain x, y, z and w number of ethylene oxide units, respectively. The sum of x, y, z and w averages 20, and a wide range of isomers is possible. For this work, the isomer having x=y=z=w=5 was chosen as reference molecule, and 10 Tween 80 molecules were inserted into the simulation box. The resulting concentration, about 32.4 mM, is higher than the critical micelle concentration (CMC), which has been reported to lie in the range 0.010-0.015 mM at 25 °C for Tween 80.[37] This is important because, if the surfactant prevents surface-induced unfolding by coating the interface and thus inhibiting protein adsorption, surfactant concentrations near or above the CMC are generally necessary to provide stabilization.

The GenIce algorithm[38] was used to obtain an initial configuration of hexagonal (Ih) ice with proton disorder and zero dipole moment, and the generated ice layer was oriented with the basal {0001} plane in the direction of the liquid phase. The silica-water interface considered in this study was hydrophilic (OH terminal group), and the same force field described in Das et al.[39] was used. The Ih ice water molecules and silica heavy atoms were kept frozen in place during the simulations. For simulating the air-water interface, a 5 nm vacuum space was included along the Z axis above the liquid phase.

The simulations were performed using periodic boundary conditions. Long-range electrostatic interactions were treated using the Particle Mesh Ewald (PME) algorithm.[40] A cut-off radius of 1.2 nm was used for both the real-space Coulombic and Lennard-Jones interactions. In all simulations, 1 native protein molecule was introduced into the simulation box, solvated with SPC/E water molecules (the number of water molecules in each simulation box is listed in Table 1), and neutralized using Na^+ ions. The liquid phase was equilibrated for 5 ns at 1 bar and 260 K in the NPT ensemble, using Berendsen pressure and temperature coupling.[41] To accelerate sampling we performed multiple-walkers (MWs)[42] PBMetaD using 3 multiple walkers. PBMetaD simulations were performed at 260 K in the NVT ensemble, with the temperature controlled by stochastic velocity rescaling.[43] We used an integration timestep of 2 fs for the MD equations of motion, and each walker was simulated in a production run

of 100 ns.

Parallel bias metadynamics

In a PBMetaD simulation several one-dimensional bias potentials $\{V(s_i)\}$ are deposited, each acting on a different CV s_i, which is a function of the atomic coordinates $s_i(\mathbf{R})$. The individual bias potentials have the familiar form of a metadynamics bias potential

$$V(s_i,t) = \int_0^t dt'\ \omega_i(t') \exp\left(-\frac{(s_i(\mathbf{R}) - s_i(\mathbf{R}(t')))^2}{2\sigma_i^2}\right) \tag{1}$$

with σ_i a Gaussian width specific to CV s_i and $\omega_i(t)$ a deposition hill height which decreases as the bias accumulates according to

$$\omega_i(t) = \omega_{0,i}\ \exp\left(-\frac{V(s_i,t)}{k_B \Delta T_i}\right) \times \frac{\exp\left(-\frac{V(s_i,t)}{k_B T}\right)}{\sum_{j=1}^{n} \exp\left(-\frac{V(s_j,t)}{k_B T}\right)} \tag{2}$$

which is the usual well-tempered[44] prescription, modified by an additional conditional probability giving a higher weight to CVs that have a lower bias potential acting on them. k_B is the Boltzmann constant; $\omega_{0,i}$ is an initial hill hight for CV s_i, and ΔT_i is an input parameter in units of temperature related to the so-called bias factor $\gamma_i = \frac{T+\Delta T_i}{T}$. The PBMetaD bias potential acting on all CVs has the form

$$V_{PB}(s_1, s_2, ..., s_n, t) = -k_B T \ln \sum_{i=1}^{n} \exp\left(-V(s_i,t)/k_B T\right). \tag{3}$$

The advantage of PBMetaD is that it allows us to include more CVs than is feasible with conventional metadynamics while still keeping to the spirit of the well-tempered approach of having a bias that becomes quasi-stationary in the long-time limit. We include up to five CVs in our PBMetaD simulations

- d: the distance between the protein center of mass (COM) and the surface. This CV

helps to sample states during the process of adsorption and has been used in a number of studies on peptide adsorption.[5,6,45]

- $\alpha\beta$: the so-called AlphaBeta similarity CV defined as

$$\alpha\beta = \sum_i \frac{1}{2}\left[1 + \cos\left(\theta_i - \theta_i^{ref}\right)\right] \tag{4}$$

where θ_i are the backbone ϕ and ψ dihedral angles and θ_i^{ref} is a reference value determined from the PDB structure. This CV allows for the conformational exploration of the protein backbone dihedral angles.[46]

- R_g: the peptide radius of gyration defined as

$$R_g = \sqrt{\left(\frac{\sum_i^N m_i|\mathbf{R}_i - \mathbf{R}_{COM}|^2}{\sum_i^N m_i}\right)} \tag{5}$$

where $\mathbf{R}_{COM}$ is the position of the center of mass. This CV helps to sample extended or compact peptide configurations.[7,46]

- β: the antiparallel β-sheet content. The native state of GB1 contains an antiparallel β-sheet; however this secondary structure may be lost upon adsorption to a surface. Biasing this CV enhances the sampling of configurations with different degrees of antiparallel β-sheet content. The antiparallel β-sheet CV is defined as the number of 3+3 residues in an antiparallel β-sheet configuration[47,48] computed as

$$\beta = \sum_\alpha g[rdist(\{R_i\}_{i\in\Omega_\alpha}, \{R^0\})]$$

where the summation runs over all possible segments involved in the antiparallel β-sheet structure, $\{R_i\}_{i\in\Omega_\alpha}$ are the atomic coordinates of a set Ω_α of six residues of the

protein, and $g(rdist)$ is a switching function

$$g(rdist) = \frac{1 - \left(\frac{rdist}{r_0}\right)^8}{1 - \left(\frac{rdist}{r_0}\right)^{12}} \tag{6}$$

A cutoff distance of $r_0 = 0.08$ nm was used, and $rdist$ is the distance RMSD with respect to a reference antiparallel β-sheet configuration $\{R^0\}$.

- CN_h/CN_t : Finally, we consider as a CV the coordination number of the Tween 80 hydrophobic tails (CN_t) or heads (CN_h) around the protein surface

$$CN = \sum_{i=1}^{N_A} \left[\sum_{j=1}^{N_B} \frac{1 - \left(\frac{r_{ij}}{r_0}\right)^n}{1 - \left(\frac{r_{i,j}}{r_0}\right)^m} \right] \tag{7}$$

where $r_{i,j}$ is the distance between species i in group A and j in group B. Group A was the protein center of mass and group B consisted of the center of masses of either the hydrophobic tail or hydrophilic head group on each surfactant molecule. We used this CV to count the number of contacts between the protein and hydrophobic/hydrophilic surfactant atoms. We set $n = 6$, $m = 12$, and $r_0 = 1$ nm.

In all PBMetaD simulations the initial Gaussian height $\omega_{0,i}$ was set to 2 kJ/mol, the bias factor γ to 10, and the Gaussian deposition rate to 1 hill/ps. The σ (Gaussian width) values used were 0.3 nm, 0.5, 0.03 nm, 0.2 and 0.7 for d, $\alpha\beta$, R_g, β and the coordination number, respectively. In the long-time limit the biases converge to $V(s_i, t \to \infty) = -\frac{\Delta T_i}{T+\Delta T_i} F(s_i) + C$ where $F(s_i)$ is the free energy as function of CV s_i and C is an irrelevant constant. Convergence was assessed by monitoring the fluctuation of the one-dimensional free energy profiles $F(s_i)$ for the different CVs during the last 10% of the simulation time (see the Supporting Information, Figures S1-S10).

A complete list of the simulations performed, in which we specify the dimensions of both the simulation box and of the liquid phase, is shown in Table 1. In simulations 1 through

8, the effect of an interface on protein stability was investigated, while simulations 9 and 10 were performed in the bulk and used as reference. In simulations 1-3 and 9, no Tween 80 molecules were introduced into the box, while, in simulations 4-8 and 10, 10 surfactant molecules were present in the liquid phase. In order to obtain meaningful information from biased simulations we need to be able to extract unbiased probability distributions which can be inverted to obtain free energies. In the context of PBMetaD we can reconstruct unbiased multi-dimensional free energy surfaces by applying the time-dependent reweighting method of Tiwary et al.[49] This reweighting method was used to obtain all of the two-dimensional free energy surfaces presented in the remainder of this work.

Table 1: Details of the PBMetaD simulations performed*.

Sim. #	Surface	# Tween 80	CVs	Box Dim., nm	Liq. Phase Dim., nm (# water mol.)
1	Air-Water	-	d, $\alpha\beta$, R_g, β	8.0 x 8.0 x 13	8.0 x 8.0 x 8.0 (20614)
2	Ice-Water	-	d, $\alpha\beta$, R_g, β	7.8 x 8.1 x 11	7.8 x 8.1 x 8.0 (17202)
3	Silica-Water	-	d, $\alpha\beta$, R_g, β	8.1 x 8.8 x 13	8.1 x 8.8 x 8.0 (23168)
4	Air-Water	10	d, $\alpha\beta$, R_g, β	8.0 x 8.0 x 13	8.0 x 8.0 x 8.0 (16360)
5	Ice-Water	10	d, $\alpha\beta$, R_g, β	7.8 x 8.1 x 11	7.8 x 8.1 x 8.0 (16605)
6	Silica-Water	10	d, $\alpha\beta$, R_g, β	8.1 x 8.8 x 13	8.1 x 8.8 x 8.0 (22696)
7	Ice-Water	10	d, $\alpha\beta$, R_g, β, CN_t	7.8 x 8.1 x 11	7.8 x 8.1 x 8.0 (16605)
8	Ice-Water	10	d, $\alpha\beta$, R_g, β, CN_h	7.8 x 8.1 x 11	7.8 x 8.1 x 8.0 (16605)
9	-	-	$\alpha\beta$, R_g, β	8.0 x 8.0 x 8.0	8.0 x 8.0 x 8.0 (16946)
10	-	10	$\alpha\beta$, R_g, β	8.0 x 8.0 x 8.0	8.0 x 8.0 x 8.0 (16360)

*300 ns simulation time

Results and Discussion

In the absence of surfactants, GB1 unfolds at the air/water and ice/water interfaces, but is stabilized in the presence of the silica surface

Simulations were first performed in the bulk as a reference point for protein conformational stability. In agreement with previous simulations (using a number of force fields),[15–18,22] GB1 adopts a hairpin structure. The free energy surface (FES) as a function of the radius of gyration R_g and the antiparallel β-sheet content β is shown in Figure S11a. The most sampled structure (A9) is a compact hairpin, with radius of gyration 0.78 nm and a large β-sheet content ($\beta = 3$). Here, as well as in the following, the protein conformations have been labeled with a letter followed by a number. The number identifies the simulation (first column of Table 1), while the letter is used to distinguish different structures within the same simulation. Letter A always corresponds to the most folded structure within each simulation.

The free energy surfaces of the peptide, in the presence of the three surfaces and in the absence of surfactant, is shown in Figure 2 as a function of antiparallel β-sheet content (β) and the distance d between the protein COM and the surface (left panel) and as a function of R_g and β (middle panel). Representative structures are shown in the right hand panel.

The protein-surface interactions were also analyzed, and the average distance from the interface for the 6 closest and the 3 furthest protein residues is shown in Figure S12.

The FES for the case of the air-water interface is shown in Figure 2a. The protein is destabilized compared to the bulk, populating conformations with low β-sheet content ($\beta = 1.25$ or 0.5, respectively for conformations B1 and C1). The most unfolded conformation (C1, also shown in the right hand panel in Figure 2a) is surface bound (less than 0.5 nm from the surface), while the native-like conformation A1 lies at distances greater than 1 nm from the surface. Analysis of the distance of the amino acids from the surface (Figure S12a) shows that the region including the hairpin turn, i.e. residues 46-51 (DDATKT), approached the

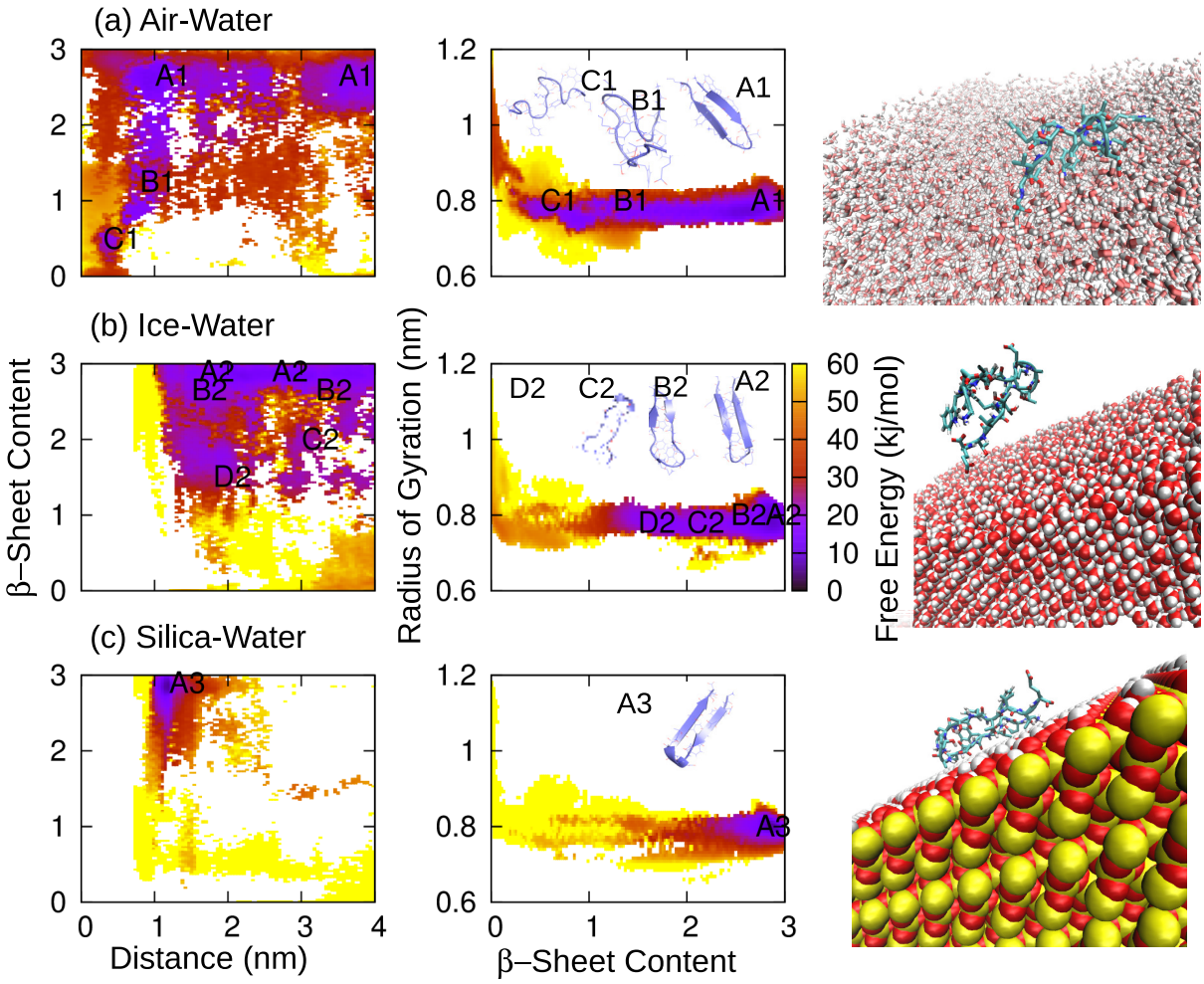

Figure 2: Free energy surface (FES) as function of distance and β-sheet content (left) or β-sheet content and radius of gyration (center) for the (a) air-water, (b) ice-water and (c) silica-water interface. On each line, a snapshot of the system being investigated is also displayed (right). The letters on the FES identify the most sampled protein conformations, and a cartoon of each structure is also shown in the β vs R_g FES. The results refer to simulations 1, 2 and 3 in Table 1, where no Tween 80 molecules were present in the simulation box.

air-water interface the most, while residues 41G, 55T and 56E were, on average, the furthest away. The amino acids that interacted with the surface, in particular residues 48-50 (ATK), showed a large increase in non-polar surface area. A significant increase in the exposed hydrophobic area was also observed for the amino acid pair 43W-54V, which is involved in the hairpin hydrophobic core. The observed loss of structure is therefore related to the adsorption of the protein at the interface, and the subsequent exposure of its hydrophobic groups to the vacuum. Indeed, structure C1 shows a larger radius of gyration ($R_g \approx 0.8$ nm) and non-polar surface area (9 nm^2) than conformation A1 (0.75 nm and 7.5 nm^2, respectively).

Interestingly, in contrast to the air-water interface, only partial unfolding of the protein is observed at the ice-water interface (Figure 2b). In fact, conformation A2 to D2 showed similar radius of gyration $R_g \approx 0.78$ nm. The least native-like conformation at the ice-water interface (conformation D2, $\beta = 1.5$), showed significantly more secondary structure than the conformation C1 sampled at the air-water surface, retaining the turn structure. The orientation of the protein to the ice surface is different than in the case of the air-water interface, with the terminal residues 41-43 (GEW) and 54-56 (VTE) now closest, and the turn residues 48A, 49T and 51T being the furthest (Figure S12b). We observed that at the ice-water surface, the hydrophobic pair formed by amino acids 43W-54V is affected by the surface, leading to partial unfolding. However, unlike the air-water interface, the ice surface does not strongly interact with the turn residues. As a result, the structures observed in the presence of ice had smaller variations in the non-polar surface area and in the radius of gyration as compared to the case of the air-water surface. Moreover, as can be seen from the FES as a function of β and distance from the surface (left handed panels), the protein does not approach the surface as closely as in the air-water case. The denaturing effect of the surface is long-ranged, with partially unfolded conformations observed 3 nm from the surface of ice (Figure 2b). This is further confirmed by the average distance between the protein residues and the surface, as shown in Figure S12b. The range of distance values explored

by the different residues during the simulation was extremely broad when compared to the case of the air-water interface (Figure S12a).

In sharp contrast to the ice-water and air-water interface, only the native structure is significantly sampled at the hydrophilic silica-water interface (Figure 2c). Comparison to the bulk FES (as a function of R_g and β-sheet content, Figure S11a) shows that the protein is in fact stabilized compared to the bulk in the presence of the silica surface. The FES as a function of β-sheet content and distance from the surface (Figure 2c) indicates that the hairpin remains near the surface, as evidenced from the small range of d (around 1 nm) sampled. The protein is oriented with the turn region, with residues 45-50 (YDDATK) towards the surface and residues 41-43 (GEW) towards the bulk (Figure S12c). Adsorption of the protein does not translate into a loss of secondary structure. It is also interesting to note that the protein approached the silica-water interface more closely than the ice-water surface, with a minimum value of the protein COM-surface distance of $d \approx 1$ nm and $d \approx 1.5$ nm for the silica and ice surfaces, respectively. In the case of the air-water interface (Figure 2a), the protein could stretch out in the vacuum, and the distance from the interface can hence be smaller than in the case of solid surfaces.

Overall, these results suggest that the unfolding process of the GB1 hairpin at the air-water interface was mainly driven by hydrophobic interactions. The denaturation process involved disruption of the hairpin turn, and exposure of residues 43W and 54V, which are part of the hydrophobic core in the native protein. A similar exposure of the hydrophobic residues 43W-54V promoted partial unfolding at the ice-water surface, however, the turn structure was retained in this case. In contrast, the GB1 hairpin was significantly stabilized by the silica-water surface, as a result of weak interactions between the protein and silica, with the surface restricting the conformations that the protein can adopt and thereby stabilizing the protein through a confinement effect.

The surfactants stabilize the protein on different surfaces to different extents and by different mechanism

We now turn to an analysis of the effect of the surfactant on protein stability. The effect of Tween 80 on the FES at the air-water, ice-water and silica-water interfaces is shown in Figure 3.

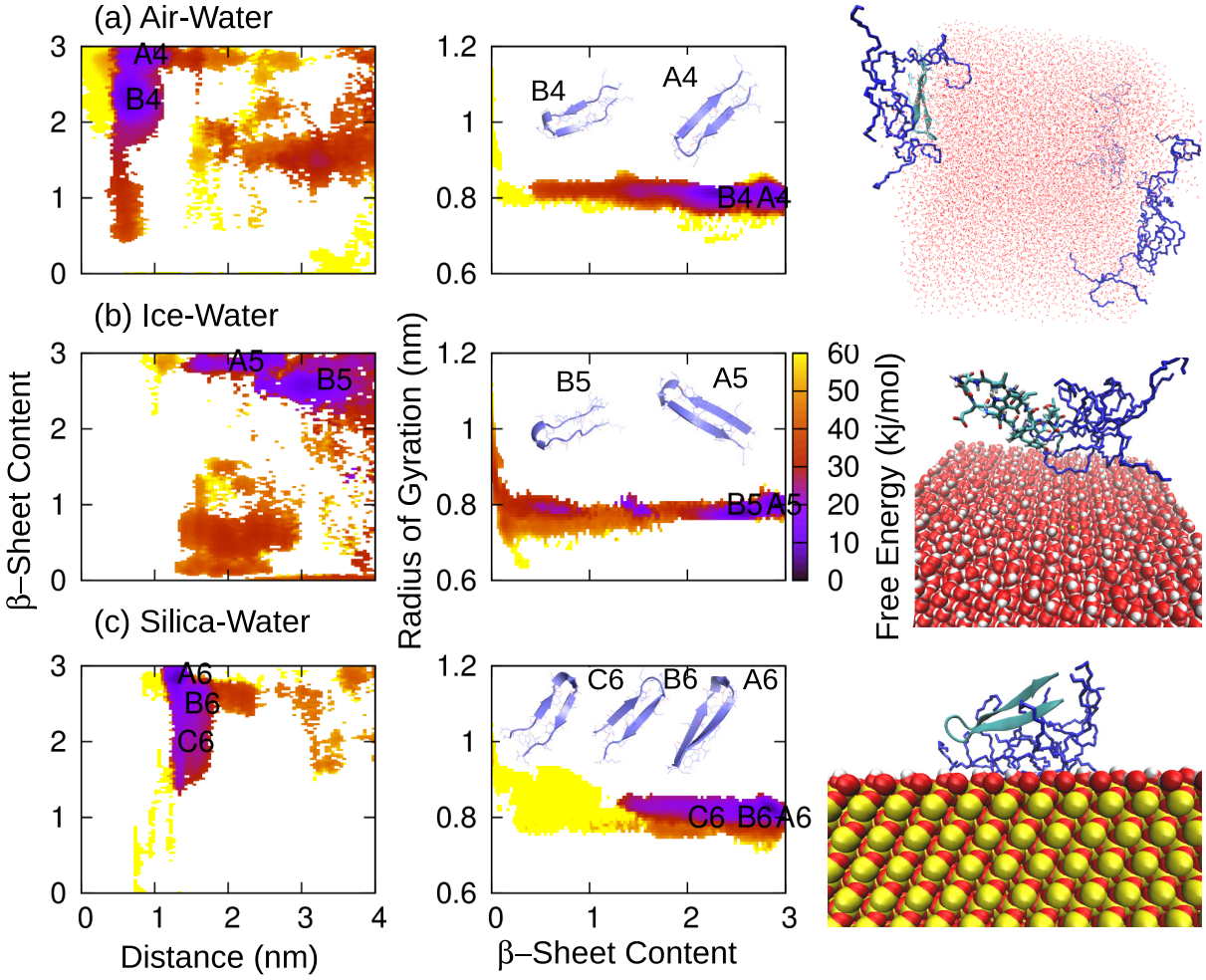

Figure 3: Free energy surface (FES) as a function of distance and β-sheet content (left) or β-sheet content and radius of gyration (center) for the (a) air-water, (b) ice-water and (c) silica-water interface. On each line, a snapshot of the system being investigated is also displayed (right), where the Tween 80 molecules are represented in blue. The letters on the FES identify the most sampled protein conformations, and a cartoon of each structure is also shown in the β vs R_g FES. The results refer to simulations 4, 5 and 6 in Table 1, where 10 Tween 80 molecules were present in each simulation box.

The surfactants stabilize the protein at the air-water interface by binding to the interface

In the case of the air-water interface (Figure 3a), the surfactant molecules were extremely effective in stabilizing the native protein conformation, with the peptide now only significantly populating structures with high β-sheet content ($\beta = 3$ or 2.3 for structures A4 and B4, respectively), and a compact radius of gyration R_g. The stabilizing effect of Tween 80 was remarkable, especially if we consider that structures A4 and B4 were more folded than the structure C9 (Figure S11a) sampled in bulk and in the absence of surfactants. It is also interesting to observe that conformation B4 showed the same radius of gyration ($R_g = 0.8$ nm) and β-sheet content ($\beta = 2.3$) as structure A10 (Figure S11b), which was the most populated in bulk upon addition of surfactants.

The surfactants bind to the surface (as shown by Figure 4a) thereby reducing adsorption of the protein at the air-water interface, as evident from the larger protein-surface distance in Figure 3a (0.5-1 nm) than in Figure 2a (structure C1 was mostly sampled at $d \approx 0.3$ nm). The protein was therefore no longer as close to the surface as in the absence of surfactants, because the Tween 80 molecules coated the interface, sterically preventing the hairpin adsorption. This significantly limited the range of d values explored by the protein, that generally remained confined between 0.5 and 1 nm from the interface (Figure 3a). In the absence of Tween 80, the protein denatured at the air-water interface because of direct interactions between the protein's hydrophobic core and the air; this process is prevented in the presence of the surfactants that preferentially bind to the interface over the protein.

The surfactants stabilize the protein at the water-ice interface through an orientation-dependent binding of the hydrophilic heads of the surfactants to the protein

The Tween 80 molecules showed a similar stabilizing effect in the presence of ice, as shown in Figure 3b. In this case, only two very compact conformations were observed, with a native-like secondary structure ($\beta = 3$ or 2.65 for conformations A5 or B5, respectively).

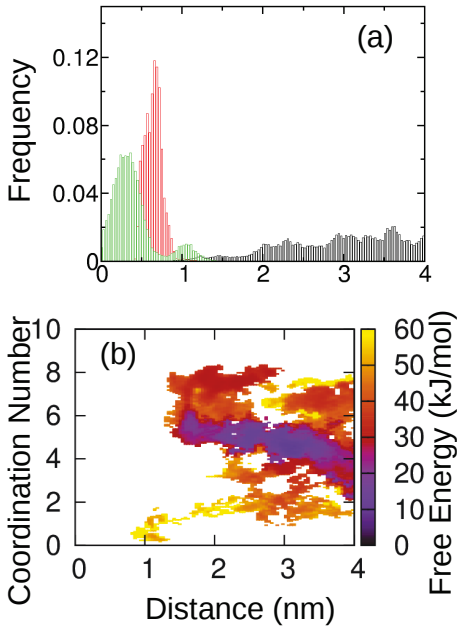

Figure 4: (a) Histogram showing the distribution of the distance between the Tween 80 molecules COM and the air-water (green bars, simulation 4), silica-water (red bars, simulation 6) and ice-water (black bars, simulation 5) interface. (b) FES showing the coordination number between the Tween 80 molecules and the GB1 hairpin as function of the distance between the protein COM and the ice-water interface (simulation 5).

The mechanism of stabilization appears to be quite different than in the air-water case, as the surfactants do not coat the interface (Figure 4a) but rather bind directly to the protein, as evident from the high (around 5) coordination number between the Tween 80 molecules and the protein (Figure 4b). The protein is further away from the surface than in the surfactant-free case, with values of d smaller than 1.5 nm rarely sampled (Figure 3b).

To further probe the nature of the binding of the surfactants to the protein, in particular the orientation (head or tail) of the surfactants with respect to the protein, we defined an orientation parameter as the ratio between the coordination number of the surfactant tails (CN_t) and surfactant heads (CN_h) around the protein,

$$\text{Orientation Parameter} = \frac{CN_t}{CN_h} \tag{8}$$

A 1 nm distance was chosen as cut-off for both coordination numbers. An orientation parameter larger than 1 indicates that the hydrophobic tails are closer to the protein surface than the hydrophilic heads, and vice versa.

The FES showing the β-sheet content as function of the orientation parameter for the ice-water simulations in the presence of surfactants is shown in Figure 5a. Native-like, compact structures (A5 and B5) are stable for values of the orientation parameter smaller than 1 (hydrophilic heads facing the peptide), while the few structures with smaller β-sheet content (primarily energetically unfavorable) were observed only when the orientation parameter was larger than 1 (hydrophobic tails facing the protein).

Therefore, this FES suggests the presence of an orientation-dependent mechanism in which the native-like structures are stabilized when the surfactant molecules orient with their hydrophilic heads towards the protein, with the opposite orientation promoting loss of structure.

To confirm the orientation-dependent mechanism, we performed 2 additional simulations (simulations 7-8 in Table 1) in which the coordination number between the surfactant hydrophobic tails (CN_t) or hydrophilic heads (CN_h) and the protein was used as a collective

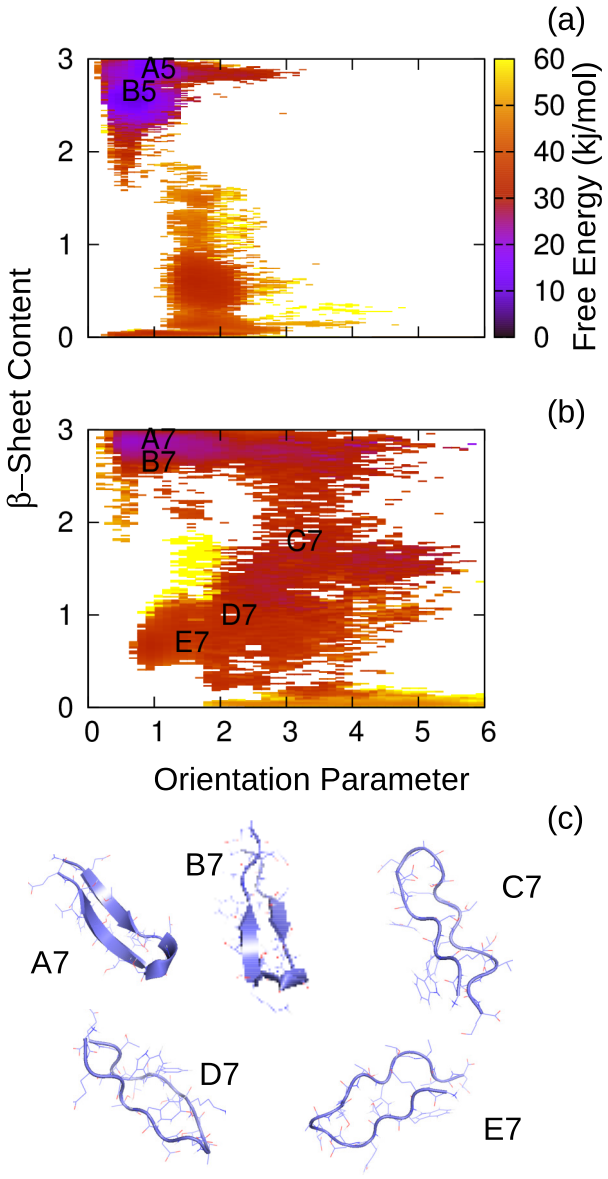

Figure 5: FES showing the hairpin β-sheet content as function of the orientation parameter during (a) simulation 5 (ice-water interface, presence of surfactants, unbiased coordination number) and (b) simulation 7 (ice-water interface, presence of surfactants, biased coordination number of surfactants tails). (c) Cartoon representations of the protein structures sampled during simulation 7.

variable in the metadynamics protocol. By biasing the coordination number CN_t, the orientation of the surfactant molecules towards the protein was also implicitly biased, promoting, in simulation 7, the tails-toward-the-protein configuration. This biasing led to the population of a large number of unfolded structures, as shown in Figure 5b (snapshots of the protein structures A7-E7 are also illustrated in Figure 5c). Structures A7 and B7 were folded ($\beta = 3$ and $\beta = 2.65$, respectively) , while structures C7 ($\beta = 1.8$), D7 (β=1) and E7 (β=0.7) showed a decreased β-sheet content. Analysis of the surfactant orientation around the protein confirmed that these unfolded structures, characterized by an almost complete loss of secondary structure, had values of the orientation parameter larger than 1 (Figure 5b). In contrast, when the coordination number of the Tween hydrophilic heads was biased CN_h, as in simulation 8, the FES was restricted towards more native conformations (Figure S13). In fact, the two most sampled conformations, A8 and B8 (Figure S13b), showed a high β-sheet content ($\beta = 3$ and 2.5, respectively). In addition to supporting an orientation-dependent mechanism, simulations 7 and 8 also show that the coordination number is not a good collective variable when the molecules involved have an amphipathic nature as the choice of CN (tail or head) influences the outcome of the simulation.

Due to their amphiphilic nature, surfactants gravitate to interfaces where there is a sharp gradient in hydrophobicity/hydrophilicity. In the case of air-water, the surfactants are strongly attracted to the interface, with the hydrophobic tails interacting with the air, and the hydrophilic heads exposed to water. Due to this preferential binding to the surface, the surfactants interact more strongly with the surface than the protein. In contrast, at the ice-water interface, while a gradient in hydrophobicity/hydrophilicity does exist, it is mild. The ice water can be considered more hydrophobic than liquid water,[50] with the water molecules having different mobilities, and different abilities to hydrogen bond. In this case, the surfactants are not strongly drawn to the interface, and preferentially coat the protein rather than the ice-water surface. Therefore, the hydrophilic heads of the surfactant face towards the protein, that exposes its hydrophilic residues in its native state.

We probed further the coordination number of the Tween 80 molecules around the peptide as it has been reported that the surfactant concentration required for protein stabilization should not correlate with the CMC when the surfactants bind directly to the protein. Rather, the degree of protection should be maximized at the molar binding stoichiometry between the surfactant and the protein.[51–53] For instance, Chou et al.[23] studied the binding of both Tween 20 and Tween 80 with Albutropin, and they reported a molar binding stoichiometry of 10:1 and 9:1 (surfactant:protein), respectively. The value of 5 that we found to be the most stable coordination number between the Tween 80 molecules and the β-hairpin in Figure 4b likely corresponds to the molar binding stoichiometry for the protein being investigated, and lies in the range of values which is experimentally observed.

The surfactants slightly destabilize the protein at the silica-water interface through an orientation-dependent binding of the hydrophobic tails of the surfactants to the protein.

In contrast, the surfactants slightly destabilize the protein at the hydrophilic silica-water interface (Figure 3c), promoting structures with smaller values of β-sheet content, with the C6 conformation, for example, having $\beta = 2$. In the absence of surfactants, as shown in Figure 2c, only the native-like conformation, characterized by $\beta = 3$, was sampled at the silica-water interface. Hence, in the case of the hydrophilic silica surface, Tween 80 promoted a partial loss of secondary structure.

The surfactants were strongly attracted to the silica-water interface, where they formed a layer of adsorbed molecules (Figure 4a). This hindered protein adsorption and increased the distance between the hairpin and the surface, as can be seen by comparing Figures 2c and 3c. A shown in the FES in Figure 6, the surfactants are oriented with their hydrophobic tails towards the protein and hydrophilic heads near the silica surface (orientation parameter larger than 1). Based on our surfactant-biased simulations at the ice-water interface,

this orientation of the Tween 80 molecules should promote the sampling of less structured conformations. The reason that the surfactants orient in this protein-unfavorable manner is because the hydrophilic heads have high affinity to the hydrophilic silica surface. As a result, only the hydrophobic tails remain available for interaction with the protein, and mild destabilization ensues.

A similar (but even milder) destabilization is observed when Tween 80 is added to the protein in the bulk (a hydrophilic aqueous environment), through the same orientation-dependent mechanism (as can be seen by comparing Figures S11a and S11b). The FES in the presence of Tween 80 populates fewer conformations with β near 3 and favors conformations (A10) with slightly lower β-sheet content ($\beta = 2.3$). The reason for this mild destabilization is the orientation of the hydrophobic tails towards the protein (orientation parameter larger than 1 in Figure S11c). As in the case of silica, the GB1 hairpin is surrounded by the hydrophobic chains of the surfactant molecules, and this promotes an increased exposure of the non-polar residues. However, the protein is more stable in the presence of the surface than in the bulk because of the confinement effect imparted by the hydrophilic surface.

Therefore, the orientation-dependent mechanism of Tween 80 can explain both the protein stabilization at the ice-water interface, and the loss of structure induced at the hydrophilic silica-water surface and in the bulk. The amphipathic nature of Tween 80 also explains the prevention of protein unfolding at the air-water surface, as the tails favorably interact with the interface, reducing protein adsorption and its deleterious effects.

Conclusions

The role of surfaces in modulating protein conformation was examined by investigating the folding of the GB1 hairpin near the air-water, ice-water and silica-water interfaces. GB1 was destabilized at the air-water and ice-water interfaces, but stabilized at the silica surface. In the case of the air-water interface, destabilization was caused by direct interaction of the

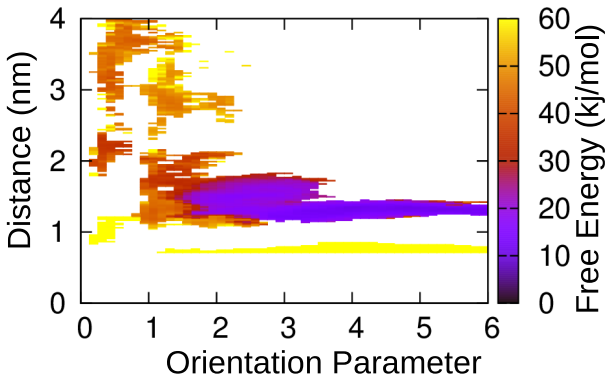

Figure 6: FES showing the relation between the orientation parameter and the distance between the protein COM and the silica-water interface (simulation 6 in Table 1).

hairpin turn and of the hydrophobic pair formed by residues 43W-54V with the vacuum. This strong interaction promoted a large exposure of non-polar surface area, and a resulting loss of structure. In the case of the ice-water surface, the interaction of residues 43W-54V with the surface promoted a partial loss of structure, but the turn structure was retained and complete unfolding was not observed. By contrast, the GB1 hairpin was stabilized at the silica surface, because of confinement effects and absence of strong protein-surface interactions.

Surfactants are commonly used in experiments to stabilize proteins in the event of surface-induced denaturation. We investigated the mechanism of surfactant action using the polysorbate Tween 80 as a model surfactant. We found that the surfactants stabilize the protein when the denaturing air-water and ice-water surfaces are present, but slightly destabilize the protein in the bulk and at the otherwise stabilizing silica interface. We observed that the surfactant molecules bind to the surface in the presence of air and silica, while they preferentially cluster around the protein in the case of ice. At the silica surface, the surfactant molecules coating the interface also directly interact with the protein, leading to mild destabilization. We identified an orientation-dependent mechanism of the surfactants, in which the protein was stabilized when the hydrophilic heads of the surfactant were oriented towards the protein, and destabilized when the hydrophobic tails pointed towards the pro-

tein. The latter orientation stabilized partially unfolded states of the protein, characterized by a larger non-polar surface area. We found that the tails-toward-the-protein configuration is favored in a hydrophilic environment, explaining the mild destabilization observed in the bulk solution, and, even more strongly, at the silica-water interface. A hydrophobic environment, on the other hand, promotes the heads-toward-the-protein arrangement, which is particularly efficient in stabilizing the protein native structure. Finally, in the case of the air-water surface, the coating of the interface by the surfactant molecules, and the resulting inhibition of protein adsorption, accounts for the observed stabilization of the protein native structure. In this case, the amphipathic nature of Tween 80 plays a major role, with the favorable interaction between the hydrophobic tails and the vacuum leading to the coating of the surface by the surfactants.

Overall, our simulations suggest that the action of surfactants is complex, as it can either stabilize or mildly destabilize the protein. The amphiphilic nature of the surfactant, and its relative affinity for the protein and the surface eventually determines the effect on the protein structure.

Acknowledgement

The authors thank Keila Cunha for providing the topology file for the silica surface. We acknowledge support from the hpc@polito team (http://www.hpc.polito.it), from the Center for Scientific Computing at the California Nanosystems Institute (CNSI), MRL: an NSF MRSEC (DMR-1720256) and NSF CNS-1725797, and we also acknowledge the CINECA award under the ISCRA initiative (ProtExc-HP10C1MQDX), for the availability of high performance computing resources and support. JES acknowledges support from the NSF (MCB-1716956) and the NIH (R01GM118560).

References

(1) Laio, A.; Parrinello, M. Escaping Free-Energy Minima. *Proc. Natl. Acad. Sci.* **2002**, *99*, 12562–12566.

(2) Valsson, O.; Tiwary, P.; Parrinello, M. Enhancing Important Fluctuations: Rare Events and Metadynamics from a Conceptual Viewpoint. *Annu. Rev. Phys. Chem.* **2016**, *67*, 159–184.

(3) Pfaendtner, J.; Bonomi, M. Efficient Sampling of High-Dimensional Free-Energy Landscapes with Parallel Bias Metadynamics. *J. Chem. Theory Comput.* **2015**, *11*, 5062–5067.

(4) Prakash, A.; Sprenger, K.; Pfaendtner, J. Essential Slow Degrees of Freedom in Protein-Surface Simulations: A Metadynamics Investigation. *Biochem. Biophys. Res. Commun.* **2018**, *498*, 274–281.

(5) Deighan, M.; Pfaendtner, J. Exhaustively Sampling Peptide Adsorption with Metadynamics. *Langmuir* **2013**, *29*, 7999–8009.

(6) Sprenger, K. G.; Pfaendtner, J. Strong Electrostatic Interactions Lead to Entropically Favorable Binding of Peptides to Charged Surfaces. *Langmuir* **2016**, *32*, 5690–5701.

(7) Sprenger, K. G.; Prakash, A.; Drobny, G.; Pfaendtner, J. Investigating the Role of Phosphorylation in the Binding of Silaffin Peptide R5 to Silica with Molecular Dynamics Simulations. *Langmuir* **2018**, *34*, 1199–1207.

(8) Ogorzalek, T. L.; Wei, S.; Liu, Y.; Wang, Q.; Brooks, C. L.; Chen, Z.; Marsh, E. N. G. Molecular-Level Insights into Orientation-Dependent Changes in the Thermal Stability of Enzymes Covalently Immobilized on Surfaces. *Langmuir* **2015**, *31*, 6145–6153.

(9) Levine, Z. A.; Rapp, M. V.; Wei, W.; Mullen, R. G.; Wu, C.; Zerze, G. H.; Mittal, J.; Waite, J. H.; Israelachvili, J. N.; Shea, J.-E. Surface Force Measurements and Simula-

tions of Mussel-Derived Peptide Adhesives on Wet Organic Surfaces. *Proc. Natl. Acad. Sci.* **2016**, *113*, 4332–4337.

(10) Garcia, A. E.; Sanbonmatsu, K. Y. Exploring the Energy Landscape of a β Hairpin in Explicit Solvent. *Proteins* **2001**, *42*, 345–354.

(11) Muñoz, V.; Thompson, P. A.; Hofrichter, J.; Eaton, W. A. Folding Dynamics and Mechanism of β-Hairpin Formation. *Nature* **1997**, *390*, 196–199.

(12) De Sancho, D.; Mittal, J.; Best, R. B. Folding Kinetics and Unfolded State Dynamics of the GB1 Hairpin from Molecular Simulation. *J. Chem. Theory Comput.* **2013**, *9*, 1743–1753.

(13) Best, R. B.; Mittal, J. Microscopic Events in β-Hairpin Folding from Alternative Unfolded Ensembles. *Proc. Natl. Acad. Sci.* **2011**, *108*, 11087–11092.

(14) Best, R. B.; Mittal, J. Free-Energy Landscape of the GB1 Hairpin in All-Atom Explicit Solvent Simulations with Different Force Fields: Similarities and Differences. *Proteins* **2010**, *79*, 1318–1328.

(15) Pande, V. S.; Rokhsar, D. S. Molecular Dynamics Simulations of Unfolding and Refolding of a β-Hairpin Fragment of Protein G. *Proc. Natl. Acad. Sci. U. S. A.* **1999**, *96*, 9062–9067.

(16) Zhou, R.; Berne, B. J.; Germain, R. The Free Energy Landscape for β Hairpin Folding in Explicit Water. *Proc. Natl. Acad. Sci. U. S. A.* **2001**, *98*, 14931–14936.

(17) Bolhuis, P. G. Transition-Path Sampling of β-Hairpin Folding. *Proc. Natl. Acad. Sci. U. S. A.* **2003**, *100*, 12129–12134.

(18) Paschek, D.; García, A. E. Reversible Temperature and Pressure Denaturation of a Protein Fragment: A Replica Exchange Molecular Dynamics Simulation Study. *Phys. Rev. Lett.* **2004**, *93*, 238105.

(19) Muñoz, V.; Henry, E. R.; Hofrichter, J.; Eaton, W. A. A Statistical Mechanical Model for β-Hairpin Kinetics. *Proc. Natl. Acad. Sci. U. S. A.* **1998**, *95*, 5872–5879.

(20) Honda, S.; Kobayashi, N.; Munekata, E. Thermodynamics of a β-Hairpin Structure: Evidence for Cooperative Formation of Folding Nucleus. *J. Mol. Biol.* **2000**, *295*, 269 – 278.

(21) Du, D.; Zhu, Y.; Huang, C.-Y.; Gai, F. Understanding the Key Factors that Control the Rate of β-Hairpin Folding. *Proc. Natl. Acad. Sci. U. S. A.* **2004**, *101*, 15915–15920.

(22) Zerze, G. H.; Mullen, R. G.; Levine, Z. A.; Shea, J.-E.; Mittal, J. To What Extent Does Surface Hydrophobicity Dictate Peptide Folding and Stability near Surfaces? *Langmuir* **2015**, *31*, 12223–12230.

(23) Chou, D. K.; Krishnamurthy, R.; Randolph, T. W.; Carpenter, J. F.; Manning, M. C. Effects of Tween 20® and Tween 80® on the Stability of Albutropin During Agitation. *J. Pharm. Sci.* **2005**, *94*, 1368 – 1381.

(24) Joshi, O.; McGuire, J.; Wang, D. Adsorption and Function of Recombinant Factor VIII at Solid-Water Interfaces in the Presence of Tween-80. *J. Pharm. Sci.* **2008**, *97*, 4741 – 4755.

(25) Krielgaard, L.; Jones, L. S.; Randolph, T. W.; Frokjaer, S.; Flink, J. M.; Manning, M. C.; Carpenter, J. F. Effect of Tween 20 on Freeze-Thawing- and Agitation-Induced Aggregation of Recombinant Human Factor XIII. *J. Pharm. Sci.* **1998**, *87*, 1597 – 1603.

(26) Kerwin, B. A.; Heller, M. C.; Levin, S. H.; Randolph, T. W. Effects of Tween 80 and Sucrose on Acute Short-Term Stability and Long-Term Storage at -20 C of a Recombinant Hemoglobin. *J. Pharm. Sci.* **1998**, *87*, 1062 – 1068.

(27) Arsiccio, A.; Pisano, R. Surfactants as Stabilizers for Biopharmaceuticals: An Insight into the Molecular Mechanisms for Inhibition of Protein Aggregation. *Eur. J. Pharm. Biopharm.* **2018**, *128*, 98 – 106.

(28) Liu, L.; Qi, W.; Schwartz, D. K.; Randolph, T. W.; Carpenter, J. F. The Effects of Excipients on Protein Aggregation During Agitation: An Interfacial Shear Rheology Study. *J. Pharm. Sci.* **2013**, *102*, 2460 – 2470.

(29) Bam, N. B.; Cleland, J. L.; Yang, J.; Manning, M. C.; Carpenter, J. F.; Kelley, R. F.; Randolph, T. W. Tween Protects Recombinant Human Growth Hormone against Agitation-Induced Damage via Hydrophobic Interactions. *J. Pharm. Sci.* **1998**, *87*, 1554–1559.

(30) Bhatnagar, B. S.; Pikal, M. J.; Bogner, R. H. Study of the Individual Contributions of Ice Formation and Freeze-Concentration on Isothermal Stability of Lactate Dehydrogenase during Freezing. *J. Pharm. Sci.* **2008**, *97*, 798 – 814.

(31) Abraham, M. J.; Murtola, T.; Schulz, R.; Pall, S.; Smith, J. C.; Hess, B.; Lindahl, E. GROMACS: High Performance Molecular Simulations through Multi-Level Parallelism from Laptops to Supercomputers. *SoftwareX* **2015**, *1-2*, 19 – 25.

(32) Tribello, G. A.; Bonomi, M.; Branduardi, D.; Camilloni, C.; Bussi, G. PLUMED 2: New Feathers for an Old Bird. *Comput. Phys. Commun.* **2014**, *185*, 604 – 613.

(33) Chris, O.; Alessandra, V.; E., M. A.; F., V. G. W. A Biomolecular Force Field Based on the Free Enthalpy of Hydration and Solvation: The GROMOS Force-Field Parameter Sets 53A5 and 53A6. *J. Comput. Chem.* **2004**, *25*, 1656–1676.

(34) Fuchs, P. F. J.; Hansen, H. S.; Hunenberger, P. H.; Horta, B. A. C. A GROMOS Parameter Set for Vicinal Diether Functions: Properties of Polyethyleneoxide and Polyethyleneglycol. *J. Chem. Theory Comput.* **2012**, *8*, 3943–3963.

(35) Gronenborn, A. M.; Filpula, D. R.; Essig, N. Z.; Achari, A.; Whitlow, M.; Wingfield, P. T.; Marius Clore, G. A Novel Highly Stable Fold of the Immunoglobulin Binding Domain of Streptococcal Protein G. *Science* **1991**, *253*, 657–661.

(36) Tang, X.; Huston, K. J.; Larson, R. G. Molecular Dynamics Simulations of Structure-Property Relationships of Tween 80 Surfactants in Water and at Interfaces. *J. Phys. Chem. B* **2014**, *118*, 12907–12918.

(37) Mahmood, M. E.; Al-koofee, D. A. F. Effect of Temperature Changes on Critical Micelle Concentration for Tween Series Surfactant. *Global. J. Sci. Front. Res. Chem.* **2013**, *13*, 1–7.

(38) Masakazu, M.; Takuma, Y.; Hideki, T. GenIce: Hydrogen-Disordered Ice Generator. *J. Comput. Chem.* **2018**, *39*, 61–64.

(39) Das, S.; Lee, B. H.; Linstadt, R. T. H.; Cunha, K.; Li, Y.; Kaufman, Y.; Levine, Z. A.; Lipshutz, B. H.; Lins, R. D.; Shea, J.-E. et al. Molecularly Smooth Self-Assembled Monolayer for High-Mobility Organic Field-Effect Transistors. *Nano Lett.* **2016**, *16*, 6709–6715.

(40) Essmann, U.; Perera, L.; Berkowitz, M. L.; Darden, T.; Lee, H.; Pedersen, L. G. A Smooth Particle Mesh Ewald Method. *J. Chem. Phys.* **1995**, *103*, 8577–8593.

(41) Berendsen, H. J. C.; Postma, J. P. M.; van Gunsteren, W. F.; DiNola, A.; Haak, J. R. Molecular Dynamics with Coupling to an External Bath. *J. Chem. Phys.* **1984**, *81*, 3684–3690.

(42) Raiteri, P.; Laio, A.; Gervasio, F. L.; Micheletti, C.; Parrinello, M. Efficient Reconstruction of Complex Free Energy Landscapes by Multiple Walkers Metadynamics. *J. Phys. Chem. B* **2006**, *110*, 3533–3539.

(43) Bussi, G.; Donadio, D.; Parrinello, M. Canonical Sampling through Velocity Rescaling. *J. Chem. Phys.* **2007**, *126*, 014101.

(44) Barducci, A.; Bussi, G.; Parrinello, M. Well-Tempered Metadynamics: A Smoothly Converging and Tunable Free-Energy Method. *Phys. Rev. Lett.* **2008**, *100*, 020603.

(45) Levine, Z. A.; Fischer, S. A.; Shea, J.-E.; Pfaendtner, J. Trp-Cage Folding on Organic Surfaces. *J. Phys. Chem. B* **2015**, *119*, 10417–10425.

(46) Prakash, A.; Baer, M. D.; Mundy, C. J.; Pfaendtner, J. Peptoid Backbone Flexibilility Dictates Its Interaction with Water and Surfaces: A Molecular Dynamics Investigation. *Biomacromolecules* **2018**, *19*, 1006–1015.

(47) Pietrucci, F.; Laio, A. A Collective Variable for the Efficient Exploration of Protein Beta-Sheet Structures: Application to SH3 and GB1. *J. Chem. Theory .Comput.* **2009**, *5*, 2197–2201.

(48) Baftizadeh, F.; Biarnes, X.; Pietrucci, F.; Affinito, F.; Laio, A. Multidimensional View of Amyloid Fibril Nucleation in Atomistic Detail. *J. Am. Chem. Soc.* **2012**, *134*, 3886–3894.

(49) Tiwary, P.; Parrinello, M. A Time-Independent Free Energy Estimator for Metadynamics. *J. Phys. Chem. B* **2015**, *119*, 736–742.

(50) Hovgaard, L.; Frokjaer, S.; van de Weert, M. *Pharmaceutical Formulation Development of Peptides and Proteins, Second Edition*; Taylor & Francis, 2012.

(51) Bam, N. B.; Randolph, T. W.; Cleland, J. L. Stability of Protein Formulations: Investigation of Surfactant Effects by a Novel EPR Spectroscopic Technique. *Pharm. Res.* **1995**, *12*, 2–11.

(52) Randolph, T. W.; Jones, L. S. *Rational Design of Stable Protein Formulations: Theory and Practice*; Kluwer Academic: New York, 2002.

(53) Deechongkit, S.; Wen, J.; Narhi, L. O.; Jiang, Y.; Park, S. S.; Kim, J.; Kerwin, B. A. Physical and Biophysical Effects of Polysorbate 20 and 80 on Darbepoetin Alfa. *J. Pharm. Sci.* **2009**, *98*, 3200 – 3217.

Graphical TOC Entry